ISBN: 978-3-95450-233-2 ISSN: 2673-5504 doi:10.18429/JACoW-SRF2021-WEPTEV011

DEVELOPMENT OF IN-SITU PLASMA CLEANING FOR THE FRIB SRF LINAC*

C. Zhang, K. Elliott, J. Popielarski, W. Hartung†, K. Saito, S. Kim, W. Chang, T. Xu
Facility for Rare Isotope Beams, Michigan State University, East Lansing, MI, USA

Abstract

Development of techniques for in-situ plasma cleaning of quarter-wave and half-wave resonator cryomodules is underway at the Facility for Rare Isotope Beams (FRIB). If SRF cavity performance degradation is seen during future FRIB linac operation, in-situ plasma cleaning may help to restore performance without disassembly of the cavities from the cryomodules for off-line cleaning. Initial bench measurements have been performed on a FRIB half-wave resonator using noble gases (Ne, Ar), with and without added oxygen gas. The plasma ignition threshold was measured as a function of gas pressure and composition. Studies of plasma cleaning efficacy were undertaken. A first plasma cleaning attempt was done on a FRIB quarter-wave resonator.

INTRODUCTION

The Facility for Rare Isotope Beams (FRIB) [1] is presently being commissioned at Michigan State University. The FRIB driver linac requires 46 cryomodules containing a total of 324 superconducting resonators. The cryomodules contain quarter-wave resonators (QWRs) and half-wave resonators (HWRs) optimized for a total of 4 different beam speeds. Long-term operation of FRIB as a user facility will require the cryomodules to run with high performance and high reliability.

As has been demonstrated at SNS, in-situ plasma cleaning is a promising method to restore the performance of a superconducting cavity without disassembly of the cryomodule for off-line cleaning [2, 3]. As such, plasma cleaning capability may be beneficial for long-term FRIB operations. A feasibility study for FRIB cryomodules indicates that plasma cleaning can be done on-line without modifications to the RF couplers or cryomodules.

This paper will cover the apparatus and methods developed for plasma cleaning bench tests; initial plasma cleaning development with a FRIB $\beta = 0.53$ HWR; a first plasma cleaning test on a FRIB $\beta = 0.085$ QWR, including before-and-after Dewar testing; and future plans.

APPARATUS AND METHODS

The gas delivery and pumping system for plasma cleaning is shown in Fig. 1. Gas from the cylinders is metered via mass flow controller valves and is then filtered upstream of the cavity. A mechanical pump is used to pump the gas out of the cavity. Some of the outgoing gas is sampled by a residual gas analyser, backed by a turbo-molecular pump. When using the RGA, the bypass valve is closed and the leak valve is adjusted to make the pressure low enough for RGA operation. Pressure gauges are included downstream of the cavity and upstream of the RGA.

We ignited the plasma with RF power applied via an input antenna designed for near-unity coupling at room temperature. We pulsed the RF power during plasma cleaning to reduce RF heating of the cavity walls and input antenna and mitigate surface oxidation. Moreover, past studies have shown that cleaning with pulsed RF is helpful for removal of hydrocarbons from both the top surface and the near surface, allowing extra time for diffusion of hydrocarbons to the surface [4].

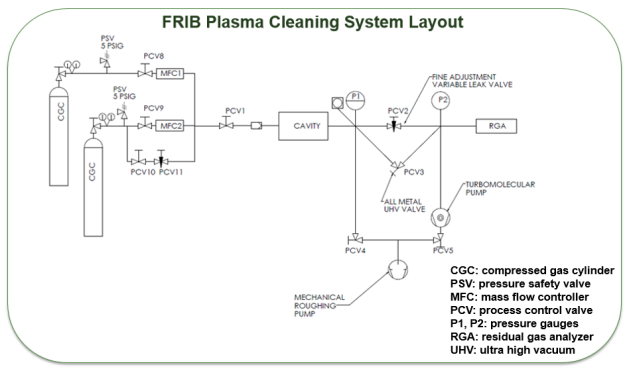

Figure 1: Schematic of gas supply and pumping system for bench plasma cleaning tests.

PLASMA CLEANING DEVELOPMENT

We did initial plasma cleaning bench tests with a $\beta = 0.53$ HWR, due to its multiple rinse ports which can be used for diagnostics (Fig. 2). HWR bench testing was done using a 100 W amplifier to excite the plasma, with an RF circuit and data acquisition system similar to that used for Dewar testing. We measured and recorded the RF power (forward, reverse, transmitted), pressures, light spectra, and RGA spectra.

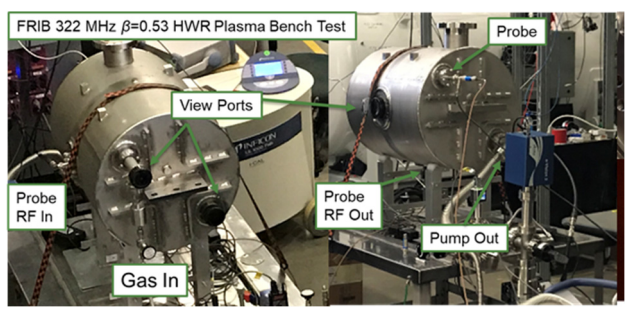

Figure 2: Bench plasma cleaning of a FRIB $\beta = 0.53$ HWR. Left: gas feed. Right: gas pumping.

*Work supported by the U.S. Department of Energy Office of Science under Cooperative Agreement DE-SC0000661.
†e-mail address: hartung@frib.msu.edu

ISBN: 978-3-95450-233-2 ISSN: 2673-5504 doi:10.18429/JACoW-SRF2021-WEPTEV011

Plasma Ignition Field

Figure 3 shows the measured RF field for plasma ignition in the β = 0.53 HWR as a function of gas pressure for different noble gases (Ar, Ne). The cavity field is inferred from the RF measurements. For Ar, the ignition threshold field first decreases rapidly and then increases gradually as a function of pressure, with a minimum at about 200 mtorr. For Ne, the threshold field decreases rapidly at low pressure as well, but no minimum is evident up to 1 torr. Due to the higher ionization energy of Ne (Ne: 21.6 eV, Ar: 15.8 eV), the threshold field for Ne is higher than that of Ar at low pressure.

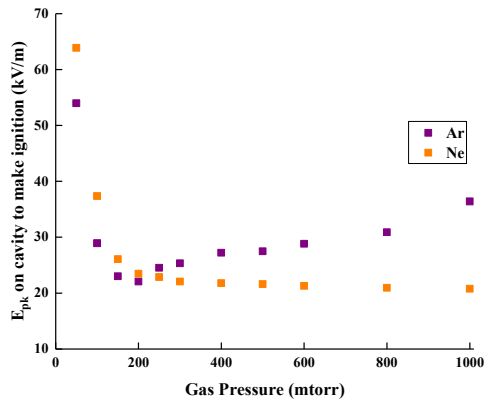

Figure 3: Dependence of the plasma ignition field for Ar and Ne on the gas pressure. E_{pk} = cavity peak surface electric field.

Optical Spectrum: Measurements

We measured the optical spectrum signal through a viewport on the cavity beam port via an optical fiber. Figure 4 shows the optical emission lines at different wavelengths for Ar (purple) and Ne (orange) plasmas at 50 mtorr gas pressure. Some of the wavelengths are given in Table 1.

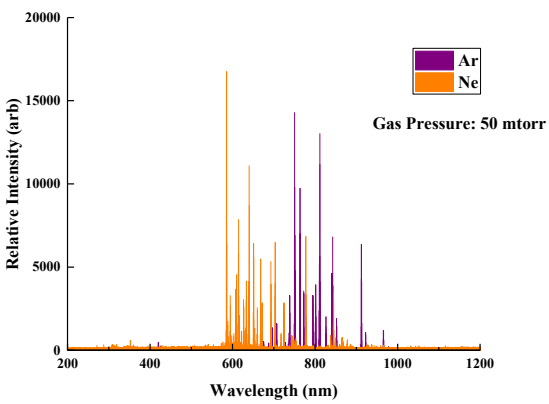

Figure 4: Optical emission spectra for Ar and Ne.

Table 1: Noble Gas Emission Spectral Lines

Source	Wavelengths (nm)
Ar	750.4, 763.5, 751.5, etc.
Ar+	426.7, 476.5, 459.0, etc.
Ne	585.2, 640.2, 614.3, etc.
Ne+	382.98, 380.0, 394.2, etc.

Optical Spectrum: Analysis

The difference in relative intensity of spectra for different excitation states can be used to estimate the electron excitation temperature and electron density. In the local thermal equilibrium (LTE) model [5], the number of excited particles follows a Boltzmann distribution, so that the electron excitation temperature T_{ext} satisfies

$$\ln\left(\frac{I_{ij}\lambda_{ij}}{A_{ij}g_i}\right) = -\frac{E_i}{\kappa_B T_{ext}} + C\,, \qquad (1)$$

where I_{ij} is the spectral line intensity, λ_{ij} is the wavelength, A_{ij} is the transition probability from (upper) level i to (lower) level j, g_i is the statistical weight, E_i is the excitation energy of level i which can be obtained from Ref. [6], and κ_B is the Boltzmann constant. Choosing several excitation levels with different E_i, we can infer T_{ext}, as shown in Fig. 5. Figure 6 shows the electron excitation temperature as function of pressure for Ar and Ne.

According to the plasma sheath model [7], the ion bombardment energy at the cavity surface is

$$\xi_{wall} = \frac{T_{ext}}{2}\left[\ln\left(\frac{M_{ion}}{2\pi m_e}\right) + 1\right], \qquad (2)$$

where M_{ion} and m_e are the ion and electron masses, respectively. Equation (2) indicates that a higher ion mass or a higher T_{ext} results in a higher ion bombardment energy. Figure 7 shows the ion impact energy as function of gas pressure calculated using Equation (2). In the 50 to 200 mtorr gas pressure range, the plasma shealth model predicts an impact energy between 3 to 4.5 eV for Ar ions and an impact energy between 5 to 12 eV for Ne ions.

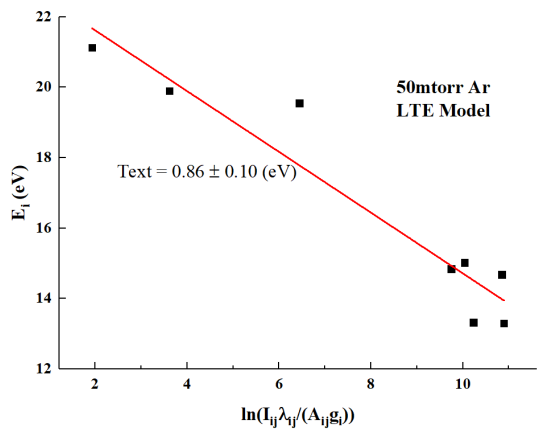

Figure 5: Fit to obtain the electron excitation temperature.

ISBN: 978-3-95450-233-2 ISSN: 2673-5504 doi:10.18429/JACoW-SRF2021-WEPTEV011

The Saha-Boltzmann Equation can be used to estimate the electron density [8]:

$$n_e = 6.04 * 10^{27} * \frac{I^*_Z}{I^*_{Z+1}} * T_{ext}^{\frac{3}{2}} * \exp\left(\frac{E_{k,z} - E_{k,Z+1} - \chi_Z}{T_{ext}}\right), \quad (3)$$

where $I^*_Z = Iz\,\lambda_{ki,Z}/(g_{k,Z}A_{ki,Z})$ and χ_Z is the excitation energy of the species in the ionization stage Z. Figure 8 shows the electron density as function of pressure calculated from Equation (3).

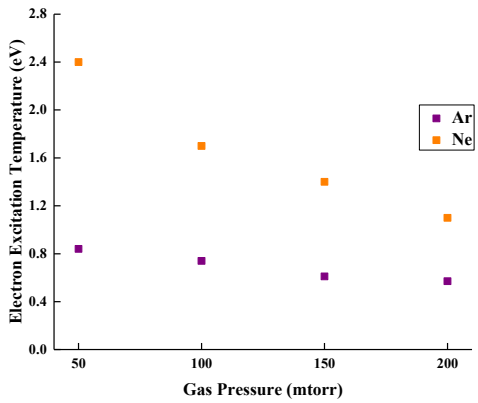

Figure 6: Calculated electron excitation temperature as a function of pressure.

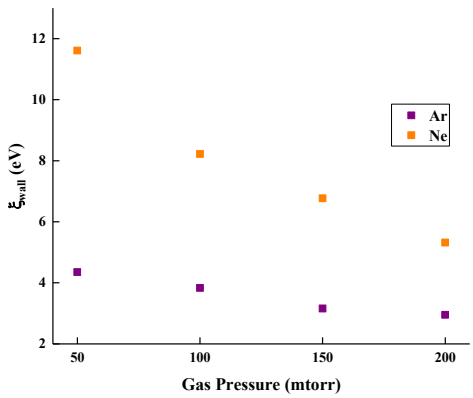

Figure 7: Calculated ion bombardment energy as a function of pressure.

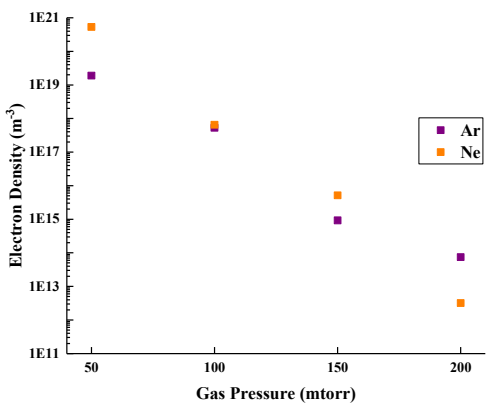

Figure 8: Calculated electron density as a function of pressure.

Noble Gas Choice

Assuming that higher ion impact energy and higher electron density allow for more effective plasma cleaning, Figures 7 and 8 indicate that Ne plasma is generally more effective than Ar, as the predicted impact energy is higher and the electron density is higher or comparable for all but the highest-pressure case.

Gas Pressure Considerations

Figures 7 and 8 predict that a lower gas pressure provides better cleaning due to higher ion impact energy and higher plasma density. Monitoring of the partial pressure of the byproducts during plasma cleaning also indicates that lower gas pressure is advantageous, as seen in Fig. 9: at 150 mtorr (red), CO is released at a greater rate when the plasma is turned on with RF pulses; at 200 mtorr (black), CO is released at a lower rate.

At very low gas pressure, we observed sputtering of copper from the input antenna onto the Nb wall of the RF port, as shown in Fig. 10. We varied the gas pressure stepwise in order to find a gas pressure which allows effective plasma cleaning without sputtering.

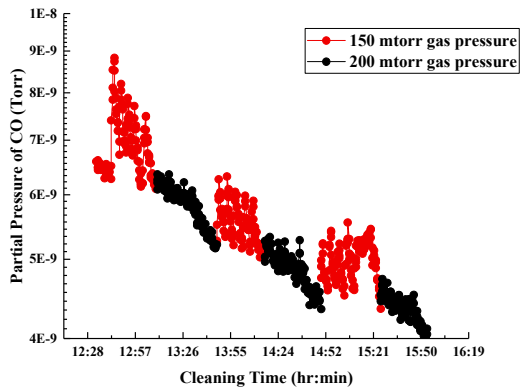

Figure 9: Measured partial pressure of carbon monoxide during plasma cleaning based on RGA spectra.

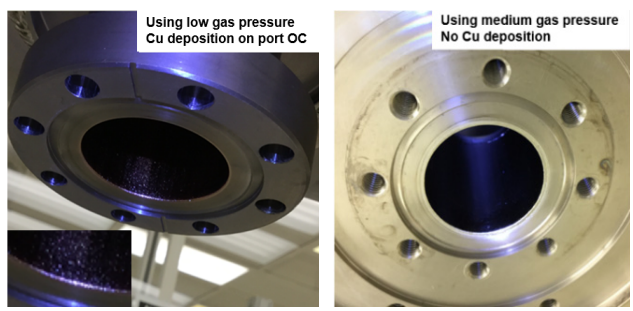

Figure 10: Left: at low pressure, sputtering of Cu is seen on the RF port. Right: at medium pressure, no sputtering is observed.

Oxygen Ratio

We tried different oxygen ratios between 1% and 10%. Based on the partial pressure of byproducts, 5% oxygen provides the most effective cleaning, as shown in Fig. 11.

ISBN: 978-3-95450-233-2 ISSN: 2673-5504 doi:10.18429/JACoW-SRF2021-WEPTEV011

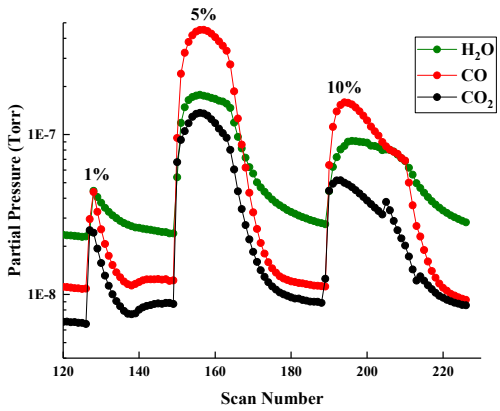

Figure 11: Partial pressures of reaction byproducts from RGA spectra with different oxygen ratios to Ne.

Pulsed RF Power for Plasma Cleaning

As described above, we modulated the RF amplitude during plasma cleaning. The RF power traces are shown schematically in Fig. 12. Ignition of the plasma produces a drop in the reverse power.

Plasma Cleaning Duration

Figure 13 shows long-term trends in the partial pressures of the reaction byproducts during plasma cleaning. A cleaning duration of order 6 to 7 hours was used based on the information from the RGA spectra.

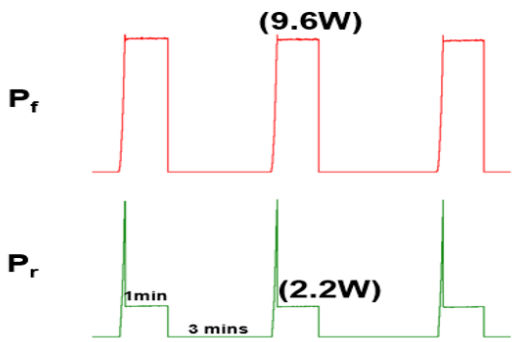

Figure 12: An example of RF amplitude modulation for Ne plasma cleaning. P_f = forward power, P_r = reverse power.

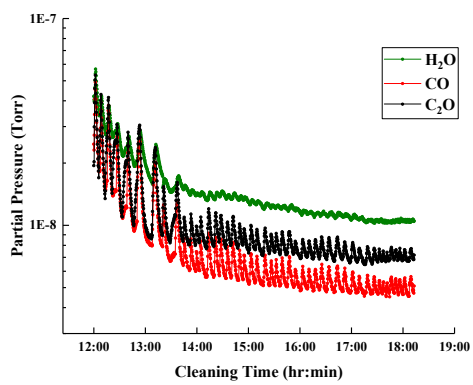

Figure 13: Partial pressures measured with the RGA during plasma cleaning.

PLASMA CLEANING OF A FRIB QWR

We applied the recipe developed in HWR plasma cleaning tests (Ne at 100 mtorr with 5% O2) to a FRIB β = 0.085 QWR, with a Dewar test before and after cleaning. The cavity chosen for plasma cleaning had some field emission X-rays in the first vertical test; it was warmed up and plasma cleaning was done using a dedicated input antenna for a good match at room temperature. As a consequence, venting of the cavity was needed before and after plasma cleaning.

Figure 14 shows the plasma cleaning setup. Figure 15 shows the Dewar test results before and after plasma cleaning. The plasma cleaning almost doubled the field emission onset and dramatically reduced the X-rays. We did not observe any degradation in the quality factor due to plasma cleaning.

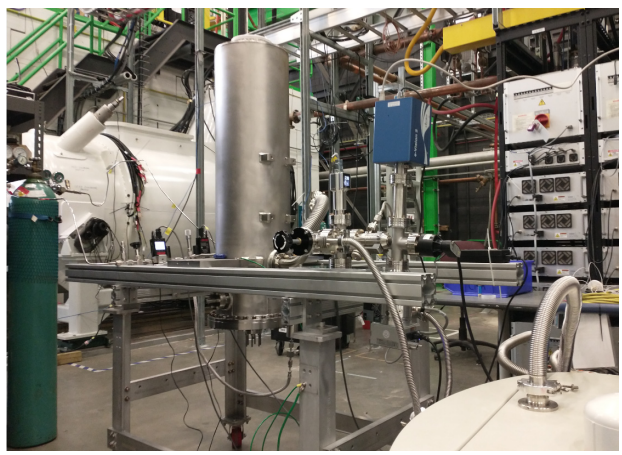

Figure 14: Bench plasma cleaning of a β = 0.085 QWR.

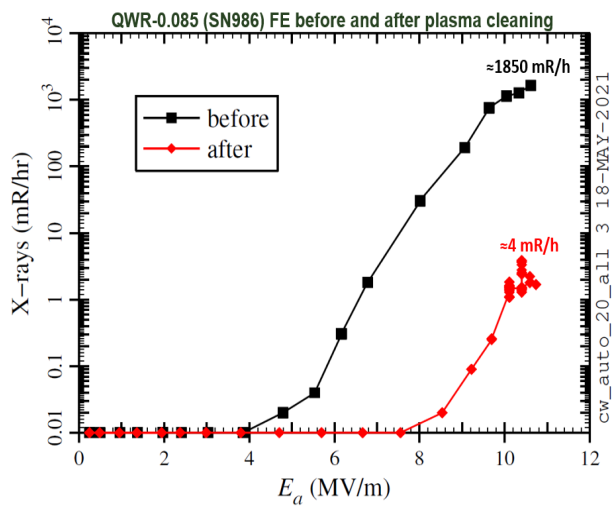

Figure 15: Field emission X-rays measured in the β = 0.085 QWR before and after plasma cleaning.

SUMMARY AND FUTURE PLANS

Plasma cleaning tests on a FRIB half-wave resonator guided our choice of gas type, gas pressure, and oxygen ratio for effective cleaning without Cu sputtering. Plasma cleaning of a FRIB quarter-wave resonator was done;

ISBN: 978-3-95450-233-2 ISSN: 2673-5504 doi:10.18429/JACoW-SRF2021-WEPTEV011

before-and-after Dewar tests show that the plasma reduced the field emission X-rays significantly. Additional plasma cleaning tests with a FRIB fundamental power coupler are planned to further develop capabilities for in-situ plasma cleaning of FRIB cryomodules.

REFERENCES

[1] T. Glasmacher *et al*., "Facility for Rare Isotope Beams Update for Nuclear Physics News", *Nuclear Physics News*, vol. 27, no. 2, 2017. https://doi.org/10.1080/10619127.2017.1317176

[2] S.–H. Kim *et al*., "Overview of ten-year operation of the superconducting linear accelerator at the Spallation Neutron Source", *Nucl. Instrum. Methods Phys. Res. A*, vol. 852, p. 20-32, 2017. https://doi.org/10.1016/j.nima.2017.02.009

[3] M. Doleans *et al*., "In-situ plasma processing to increase the accelerating gradients of superconducting radio frequency cavities", *Nucl. Instrum. Methods Phys. Res. A*, vol. 812, p. 50-59, 2016. http://dx.doi.org/10.1016/j.nima.2015.12.043

[4] P. V. Tyagi *et al*., "Improving the work function of the niobium surface of SRF cavities by plasma processing", *Appl. Surf. Sci.*, vol. 369, p. 29-35, 2016. https://doi.org/10.1016/j.apsusc.2016.02.030

[5] H. R. Griem, *Principles of Plasma Spectroscopy*, Cambridge University Press, 1997, p. 279.

[6] Atomic Spectra Database [OL], from: https://www.nist.gov/pml/atomic-spectra-database

[7] M. A. Lieberman and A. J. Lichtenberg, *Principles of Plasma Discharges and Materials Processing*, John Wiley & Sons, 2005.

[8] V. K. Unnikrishnan *et al*., "Measurements of plasma temperature and electron density in laser-induced copper plasma by time-resolved spectroscopy of neutral atom and ion emissions", *Pramana—Journal of Physics*, vol. 74, p. 983-993, 2010. http://dx.doi.org/10.1007/s12043-010-0089-5